

Dynamics of three-dimensional stepped cracks, bistability, and their transition to simple cracks

Meng Wang¹,¹ Mokhtar Adda-Bedia²,² and Jay Fineberg^{1,*}¹The Racah Institute of Physics, The Hebrew University of Jerusalem, Jerusalem 91904, Israel²Université de Lyon, Ecole Normale Supérieure de Lyon, CNRS, Laboratoire de Physique, Lyon F-69342, France (Received 1 February 2022; revised 10 May 2022; accepted 7 November 2022; published 9 January 2023)

Slow cracks may be simple, with no internal structure. The leading edge of a simple crack, the crack front, forms a single fracture plane in its wake. Slow cracks may also develop segmented crack fronts, each segment propagating along a separate fracture plane. These planes merge at locations that form steps along fracture surfaces. Steps are not stationary, but instead propagate within a crack front. Real-time measurements of crack front structure and energy flux reveal that step dynamics significantly increase energy dissipation and drastically alter crack dynamics. Simple and stepped cracks are each stable. By extending the use of energy balance to include 3D crack front structure, we find that, while energy balance is obeyed, it is insufficient to select the energetically favorable crack growth mode. Transitions from stepped cracks to simple cracks occur only when their in-plane front lengths become equal and a perturbation momentarily changes step topology. Such 3D crack dynamics challenge our traditional understanding of fracture.

DOI: [10.1103/PhysRevResearch.5.L012001](https://doi.org/10.1103/PhysRevResearch.5.L012001)

Cracks generally cause materials to fail, as they strongly amplify any remotely imposed stresses at their leading edge. Linear elastic fracture mechanics (LEFM) predicts that mathematically singular stresses will develop, in effectively 2D materials, at a crack's tip [1,2]. Crack propagation ensues via “energy balance”; when the elastic energy released per unit crack advance (energy flux into a crack's tip), G , is balanced by the fracture energy, Γ , the dissipated energy per unit crack advance. G is often called the energy release rate.

Let us now define a “simple” crack as a crack having no secondary structure [3]; a simple branch cut in 2D materials. In real 3D materials, a singular crack tip becomes a singular crack front that extends across the sample thickness, normal to the propagation direction. Simple cracks in 3D, like their 2D analogs, have no internal structure; they are invariant to translation along the crack front. So long as this invariance is not broken [4], 2D theories will fully describe their motion [1,5] and structure [6]. Simple cracks produce featureless, mirror-like, fracture surfaces.

Crack fronts are, however, not necessarily simple. Crack fronts may contain nontrivial, often dynamic, internal structures that, in their wake, create nontrivial structure on fracture surfaces [7–10]. This structure is generally accompanied by strongly enhanced dissipation. Within rapidly propagating crack fronts, complex structure may develop dynamically [7–9] as a result of a simple crack's instability to short-lived frustrated crack branching. This instability takes place at velocities that are a significant fraction of c_R , the Rayleigh wave speed.

“Stepped cracks”, as shown schematically in Fig. 1(a), are a very different type of nontrivial crack front. Stepped cracks are formed immediately upon crack initiation, when materials are subjected to small (even infinitesimal) antiplane shear (Mode III) in addition to the dominant tensile (Mode I) loading [11,12]. Such mixed mode loading excites an unstable helical mode within the crack front [13,14] that causes a single crack front to break up into separate segments. Let us define the x , y , and z directions as, respectively, the propagation, crack opening, and sample thickness directions. Each crack front segment will propagate within an xz plane that is slightly offset in y . Segmented crack fronts thereby form, in their wake, fracture surfaces that are separated in y , and slightly overlapping (in z). The segmented fracture planes, within their overlapping regions, will merge at distinct “step locations” in z , thereby forming steps on the resulting fracture surface. We define the distance, h , between these separated planes as the “step height”.

Step locations are not stationary, but move within slowly ($v \lesssim 0.1c_R$) propagating crack fronts. This motion produces faceted fracture surfaces in amorphous materials [15–17]. Studies in hydrogels revealed that steps that are oriented about $\pm 45^\circ$ to the crack's propagation direction possess the distinct, characteristic 3D structure [18] described in Fig. 1(a). They are topologically stable once formed [18]; so long as this topology is not broken, steps will stably propagate.

Once steps are formed, cracks will exhibit complex dynamics that result from energy balance coupled to the 3D dynamics within crack fronts [19]. To understand their dynamics, the full 3D structure of the crack front must be considered. Energy balance is a local concept; for a crack to propagate, G must equal the fracture energy Γ at each point z within the front. Both G and Γ are generally dependent on a crack's local speed $v(z)$. Energy balance is only realized when the internal structure of the crack front is correctly accounted for [19], as internal structure governs local energy dissipation.

*jay@mail.huji.ac.il

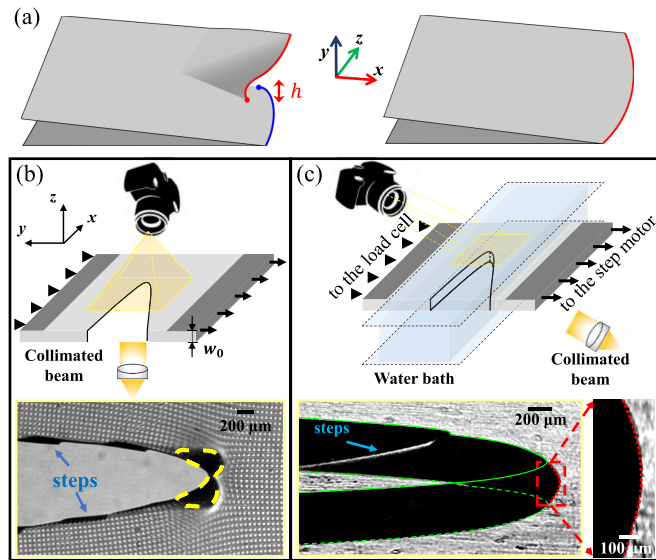


FIG. 1. Stepped and simple cracks and how they are visualized (a) Schematic diagrams of stepped (left) and simple (right) cracks. Stepped cracks are formed by segmented fronts (blue and red lines) separated by a small gap, h . The leading front (blue) is flat, while the trailing front (red) curves to merge with the leading front, defining a step's location. Cracks are visualized using two experimental setups with gel samples surrounded by either air or water. (b) In air, shadowgraph imaging of the fracture process was obtained using a collimated beam normal to the sample surface. Bottom: A step-forming crack. Lensing due to contracting material in z near the crack tip creates black caustics (yellow dashed curves). (c) Surrounding the crack with (index matching) water enables crack front visualization, when imaged obliquely. Bottom: Oblique view of an initially stepped crack that transitioned to a simple one. The crack front (red), crack tip openings on the upper ($z = w_0$, green line) and lower ($z = 0$, green dashed line) surfaces, and step created on the fracture surface (arrows) are identified. (Right) Simple crack front shape in the xz plane.

Variations in crack front structure will, thereby, induce strong variations in both Γ and $v(z)$.

Here we will focus on the dynamics and stability of stepped crack fronts. Once steps are excited on a crack front, crack front dynamics will change dramatically. Despite their topologically enforced stability [18], once $v \sim 0.1c_R$, simple crack fronts are generally observed experimentally in both gels [4,5,20] and other brittle materials [2,21] until dynamic instabilities develop at higher v . How are these observations compatible with the fact that, generically, stepped cracks are formed upon initiation, unless stringent protocols to suppress mixed mode loading [19] are enforced?

Our experiments were conducted using brittle polyacrylamide hydrogels composed with a 13.8% (w/v) acrylamide/bisacrylamide concentration and a 2.6% (w/v) crosslinker concentration. Both the viscoelastic and poroelastic effects in these gels are negligible for the time scales that we will consider [22–24].

As these gels have a Rayleigh wave speed of $c_R = 5.5 \pm 0.15$ m/s, they are ideal for studying fracture in “slow motion”. The fracture dynamics of these gels are identical to those in other brittle materials, and are well-described by

LEFM [4,5,21]. In particular, the crack tip opening displacement is well described by a parabolic shape away from the tip region, whose curvature is (see Ref. [25]) as predicted by LEFM [1,19].

The condition of small-scale yielding is well satisfied for these gels, however the physics that are taking place in the dissipative region that give rise to velocity dependence of Γ (see Fig. S4 in [25]) are still unclear [19]. This dependence may be due to poroelastic or viscoelastic effects [26–28]. While nonlinear elastic effects do, in general, occur in the close vicinity of the tip [6], for the slow velocities considered here, the size of the nonlinear region is below a single grid spacing. Moreover, the dissipative zone near the crack tip is yet smaller, which is $<20 \mu\text{m}$ for these gels [29].

In Figs. 1(b) and 1(c) we present a schematic description of our experimental system. The experiments utilized gel sheets of strip geometry ($x \times y \times z$ dimensions of $40 \times 20 \times w_0$ mm), whose unstrained thickness, w_0 , varied between 1, 0.5, and 0.25 mm. Samples were loaded in mode I by slow (strain rate $\sim 10^{-3} \text{s}^{-1}$) and uniform displacement along y until fracture initiated. Both the displacement and force are measured. Strain at fracture was controlled by the initial “seed” crack, imposed at $x = 0$ at the center in y of each sample. Seed cracks of lengths ranging from 4–6 mm yielded 6%–10% strains at fracture. Any slight tilt ($\sim 1^\circ$) of seed cracks relative to the xz plane will create steps [11]. We monitored crack dynamics (in the x direction) in areas ($\Delta x, \Delta y$) of either (10.6, 6.0) mm or (6.2, 3.5) mm, that were centered a few mm's beyond the seed crack. Crack dynamics and the near-front fields were visualized by illuminating this area with a pulsed (1 μs pulse duration) collimated (LED) beam directed into a fast camera operated at frame rates between 7000–8000 Hz with 1920×1080 pixel resolution.

We performed two types of measurements, the first with gel samples surrounded by air and the visualization direction normal to the xy plane [Fig. 1(b)]. As in [19,30], deformation fields around the crack tip were measured by the deformation of a grid mesh of $50 \times 50 \text{mm}^2$ unit imprinted on the gel's upper surface. In the near-tip singular region, the large deformations coupled with volume conservation (gels are incompressible) caused significant material contraction in z . The resultant lensing of the incident light created black caustics [9,31] near crack tips [Fig. 1(b)]. The existence of caustics prevents measurement of the grid deformation in regions adjacent to crack tips. When existent, we used caustic centroids to define crack propagation distances and mean velocities $v(t) = \langle v(z, t) \rangle_z$.

When crack front structure is created, to measure detailed dynamics of crack fronts in z , it is imperative to eliminate the caustics. To this end, we immersed the gels in a water bath and performed a second type of measurement [Fig. 1(c)]. As water is nearly index matched to the (aqueous) gel used, immersion eliminates caustics by preventing lensing of the light passing near the tip. We visualized crack front dynamics by illuminating the crack front at an oblique angle of 45° relative to the xy plane. The illuminating beam was oriented normal to x (see [25] for more details) and the transmitted light was imaged by the camera. In the measurement frame, for $w_0 = 1$ mm, sample thicknesses contracted in z to $w = 0.893 \pm 0.05$ mm. As simple crack fronts were curved, their

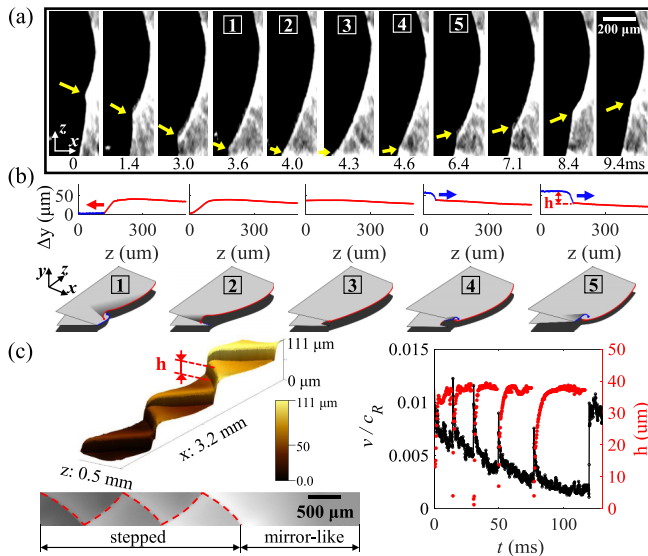


FIG. 2. Step reflections at free boundaries. (a) Sequence of in-plane crack fronts bracketing a step reflection ($w_0 = 1$ mm). Arrows denote step locations. (b) (top) Measured fracture surfaces of frames [1]–[5] in (a) and (bottom) Schematic drawing of crack fronts. (c) Left: profilometer measurements of the fracture surface of a step undergoing five reflections prior to its transition to a mirror-like simple crack (top in 3D, bottom xz plane). Right: $v(t)$ and step height, $h(t)$, dynamics for the five step reflections prior to transitioning to a simple crack.

integrated lengths, l_s , surpassed w and were nearly constant; $l_s \approx 0.945 \pm 0.03$ mm. For each w_0 used, simple crack fronts were self-similar when scaled by w_0 [25].

Stepped cracks generally develop multiple steps at initiation that coarsen or disappear upon subsequent interaction to a single step in thin sheets [19]. We focus on crack fronts containing only a single step. Fracture behavior was characterized by coupling crack front measurements with post-mortem profilometric analysis of fracture surfaces (Fig. 2). As shown in Fig. 1(a), single steps are formed by the overlap of disconnected straight and curved segments within the front [18,19]. As the overlapping section has significantly larger dissipation than other parts of the front, it locally lags behind, and forms cusp-like shapes within crack fronts in the xz plane. Step locations were identified by cusp locations [see Fig. 2(a)].

Steps may reflect when encountering a free surface (e.g., $z = 0$ or $z = w$). Figures 2(a) and 2(b) describe a step’s reflection from $z = 0$. In Fig. 2(b) we compare a step’s dynamics and instantaneous front shapes with profilometric measurements of the step height, $h(t)$ corresponding to the same instants in time. A step will always propagate in the direction (in z) that will shorten its straight segment. As demonstrated in the frames labeled [1]–[5] in Fig. 2, as the step approaches $z = 0$, (1) the straight segment shortens and (2) disappears when the lagging curved branch impinges on the free surface. At this point (3), the endpoint (in y) of the curved segment (the step location) is bent out-of-plane and, itself, becomes locally loaded under I+III mixed mode conditions. This bent section then overshoots to $h > 0$. We believe that this local mode I+III loading gives rise to a local front segmentation that, consequently, (4) creates a new step having the opposite

orientation. This “reflected” step then propagates in the opposite direction while (5) growing in height.

At each reflection, steps first lose height and then regrow while propagating. The step height h starts from a few μm until stabilizing at $h = h_{\text{max}} \approx 38 \pm 3$ μm (Fig. 2(c), right). Propagating steps trace lines, “step lines”, within fracture surfaces. Step lines bound fracture planes (“facets”) having different heights. Repeated reflections form periodic step lines, tilted approximately $\pm 45^\circ$ relative to x and create climbing facets in y , as shown in Fig. 2(c), left.

Steps lead to increased local energy dissipation by increasing 3D crack lengths by $l^{\text{step}}(t) \approx 1.4h(t)$, (which includes both their height in y and overlapping regions in z) [18]. Hence, as steps grow with propagation, their mean front speeds, $v(t)$, decrease. At the instant of each reflection, momentarily $h(t) \approx 0$ and $v(t)$ instantaneously jumps. $v(t)$ therefore oscillates in phase with repeated step reflections (Fig. 2(c), right). Over time, however, the mean value of $v(t)$ “mysteriously” decreases. Step reflections continue until, as at $t = 120$ ms in Fig. 2(c), instead of reflecting, a step disappears upon encountering a free surface. At this point, fronts transform to simple cracks and $v(t)$ consequently undergoes an instantaneous jump to a higher speed v_s . After this transition, crack fronts may either slowly accelerate or even propagate at nearly steady-state speeds.

Let us first consider the energy flux, G , into stepped crack fronts. At each instant, we calculate G via J -integrals derived using measured deformation fields. This calculation is valid since elastic fields are effectively 2D for contours located at distances much greater than w_0 . This calculated value of G is, indeed, equal to that obtained by means of the strip geometry of the experiment as in, e.g., [5].

Figures 3(a) and 3(b) present two typical examples of stepped cracks undergoing multiple step reflections before transitioning to simple cracks. Surprisingly, G is constant in time regardless of the extremely unsteady motion of the crack fronts.

We now consider the total dissipation of the stepped crack. We define $\tilde{\Gamma}$ as the total dissipation integrated over the whole crack front length l ,

$$\tilde{\Gamma} = \int_{l(t)} \Gamma(v(z, t)) dz \approx \Gamma(v(t)) \cdot l(t). \quad (1)$$

$\tilde{\Gamma}$ has units J/m and differs from the fracture energy, $\Gamma(v)$ (dissipation per unit area) which is a characteristic material property. $\Gamma(v)$ can be measured; for $v \lesssim 0.1c_R$, $\Gamma(v)$ is a nonlinear, strongly increasing function of v [19]. On the other hand, $\tilde{\Gamma}$ depends extensively on both crack front dynamics and the total instantaneous length $l(t) = l^{xz}(t) + l^{\text{step}}(t)$. The in-plane (xz plane) crack front lengths, $l^{xz}(t)$, are measured directly [see Fig. 3(c)]. Out-of-plane lengths, $l^{\text{step}}(t) \approx 1.4h(t)$, are obtained by post-mortem measurements of $h(t)$.

By energy balance, $\tilde{\Gamma} = G \cdot w$ [25]. Since G is constant, any variation of $l(t)$ immediately causes a consequent variation of $v(t)$. Thus, $v(t)$ oscillates sharply with periodic step reflections. Moreover, the continuous decrease of $v(t)$ from one reflection to the next [as in Figs 2(c) and 3(a)] implies that, beyond the periodic variations caused by $l^{\text{step}}(t)$, $l(t)$ grows with t . The continuous decrease of $v(t)$ continues until

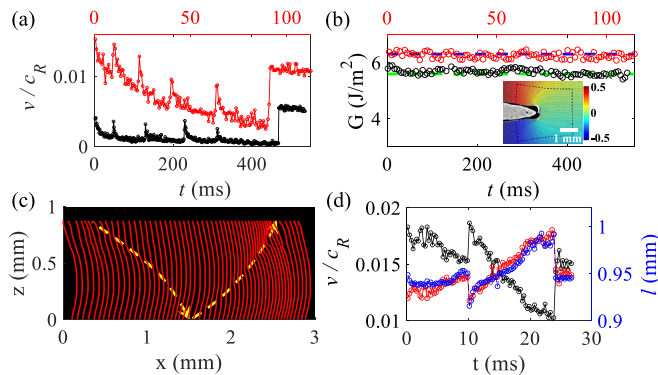


FIG. 3. Energy flux and dissipation during crack motion. (a) $v(t)$ of two stepped cracks. $v(t)$ oscillates in phase with step reflections while decreasing in time. Both examples transition to simple cracks; $v(t)$ jumps when steps disappear. (b) Despite the strong variations in $v(t)$, the corresponding energy fluxes $G(t)$ are constant. For each of the time series in (a) we present G as calculated using the J integral for each time (symbols). These values are identical to calculated values of G obtained using the strip geometry (dashed lines). Colors are as in (a). Inset: u_y in mm^2/s . Dashed line is the contour used in the J-integral calculation of G at $t = 400$ ms for black symbols. (c) Instantaneous crack fronts, separated by 0.714 ms, as a step propagates from $z = w$, reflects at $z = 0$ and then transitions to a simple crack when the step returns to $z = w$. (d) Corresponding $v(t)$ (black) and $l(t)$. (blue) Measured $l(t)$ and (red) $l(t)$ derived via energy balance are indistinguishable.

a transition to a simple crack takes place. At this point, $v(t)$ jumps sharply.

To understand both the slow variation of $v(t)$ as well as the loss of step stability, we consider in Figs. 3(c) and 3(d) the detailed dynamics of $v(t)$ and $l(t)$ of a stepped crack front as it approaches the transition to a simple crack. The in-plane crack front profiles [Fig. 3(c)] continuously vary as the step first reflects at $z = 0$ ($x = 1.5$ mm) then dies at $z = w$, upon transition ($x = 2.5$ mm) to a simple crack. Figure 3(d) shows that the measured $l(t)$ continuously increases while the entire crack front continuously slows, until the sudden transition to a simple crack.

When measured values of $l^{xz}(t)$ are not available, $l(t)$ can be derived using $l(t) = G \cdot w / \Gamma(v(t))$. Figure 3(d) demonstrates that derived values of $l(t)$ are identical to measured ones, an additional validation of energy balance. This enables us to reliably derive $l(t)$ in gels bounded by air [Fig. 1(a)], when direct measurements are impossible.

Figures 4(a) and 4(b) present the dynamics and $l(t)$ evolution of numerous cracks during successive step reflections. Figure 4(b) demonstrates that, regardless of the crack dynamics, $l(t)$ continuously increases, until a critical length of about 5.7% above the simple crack length, l_s . After reaching this length, when a step reaches a free surface (noted at $t = t^*$), instead of reflecting it disappears and $l(t)$ drops instantaneously to l_s . The drop in $l(t^*)$ [in Fig. 4(b) ~ 53 μm] corresponds precisely to the excess front length contributed by steps ($l_{\text{max}}^{\text{step}} = 1.4h_{\text{max}}$). Thus, as Fig. 4(c) demonstrates, transitions to simple cracks only occur when $l^{xz}(t) = l_s$ [25]. This transition is independent of G and w_0 .

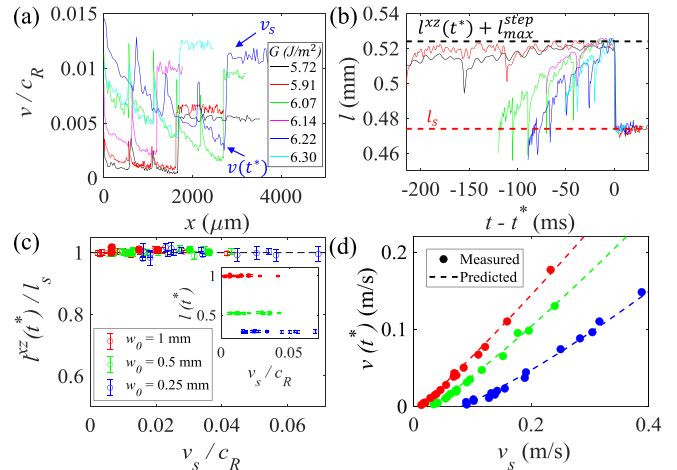


FIG. 4. Front dynamics are strongly coupled to the lengths of stepped crack fronts. (a) Crack dynamics during successive step reflections for eight experiments performed in air with $w_0 = 0.5$ mm. (b) The evolution of the derived $l(t)$ from the experiments shown in (a). The stepped cracks transition to simple cracks upon arriving at a free surface at $t = t^*$ only when $l(t)$ grows to a critical length. (c) In-plane crack front length at the transition, $l^{xz}(t^*)$, normalized by the simple crack length, l_s . Filled (open) symbols are directly measured (derived) values from experiments in water (air). Inset: Un-normalized $l(t)$ at transition for different w_0 . (d) Stepped crack velocities, $v(t^*)$ at transitions vs. simple crack velocities after transition, v_s . Predictions (dashed lines) agree perfectly with measurements (points). Colors as in Fig. 4(c).

As G is constant, at the transition to a simple crack $v(t)$ correspondingly jumps. The velocity at the transition, $v(t^*)$, is predicted by energy balance via,

$$l(t^*) \cdot \Gamma(v(t^*)) \equiv (l_s + l_{\text{max}}^{\text{step}}) \cdot \Gamma(v(t^*)) = l_s \cdot \Gamma(v_s) \quad (2)$$

with $\Gamma(v)$ shown in [25], Fig. S4. The predicted velocity at transition, $v(t^*)$, perfectly corresponds to experimental measurements, as shown in Fig. 4(d) for numerous experiments and different w_0 .

The topological constraint imposed by a step can force a crack to arrest, even if G is sufficiently large to enable the propagation of a simple crack [25]. As $l(t)$ lengthens, $v(t)$ may decrease to zero before the step arrives at a free surface. Under these circumstances, the transition to a simple crack can not take place, and a stepped crack will simply arrest. This is demonstrated in Fig. 4(d) as well as in [25]. Thus, v_s corresponding to $v(t^*) = 0$ is the minimum v_s possible for the transition from a stepped to a simple crack. This minimum value is strongly dependent on w_0 for thin sheets.

Stepped cracks and simple cracks are truly bistable modes of fracture. For example, for the values of G where $v(t^*) = 0$, if a simple crack is initiated, it will stably propagate for all velocities below the micro-branching threshold [19]. This bistability results from the topological constraints imposed on stepped cracks. Stepped cracks can not transition to simple cracks, unless a perturbation is encountered that momentarily breaks this topological constraint. This is what takes place at a free boundary—without such a “topological” perturbation, stepped cracks would either continue uninterrupted or arrest.

Since, at fracture onset, any small mode I+III mixity will create steps, we might expect that amorphous materials may all exhibit slow “topologically” creeping regimes at the onset that will “mysteriously” spontaneously jump to dynamic velocities. Such velocity jumps are, in fact, often observed in the range of materials [2,32] in which facets are observed. Our observation which shows that the step reflection will take place unless $l^{xz} = l_s$ is intriguing. $l > l_s$ in *all* of the crack lengths enclosed within the dashed lines in Fig. 4(b). Despite the successive reflections that each stepped crack undergoes, these cracks remain stable to simple cracks so long as $l^{xz} < l_s$.

Why is the crack front length of simple cracks, l_s , significantly larger than the sample width, w ? We see [Fig. 3(c)] that the shape of the crack front is significantly affected by the free surfaces, which seem to induce crack front curvature. Figure S2 [25] shows that the simple crack profiles superimpose, when scaled by w , for the thin gel samples that we have used for this study.

When a step appears, $l^{xz} < l_s$ because the cusp created by a typical step will tend to flatten the crack front over a spatial extent (in z) of $\delta z \sim 200\text{--}300\ \mu\text{m}$ [18]. As δz is on the order of w , it is not surprising that both $l^{xz} < l_s$ and that the entire front shape near the time of step “reflection” is influenced by step dynamics (for the nearly quasistatic values of $v \ll c_R$ in this regime). What is surprising is that l^{xz} grows, from reflection to reflection [Figs. 3(d) and 4(b)]. It is this growth that enables the transition [Fig. 4(c)] to simple cracks.

When w becomes much larger, it is not clear that the simple crack profile scaling shown in Fig. S2 will continue to hold. It is, however, reasonable that a *single* step will have a much smaller influence over the entire crack front, when $\delta z \ll w$. In these cases, we might expect reflections to be rare at a free surface. Empirically, this seems to be true [33].

The constantly varying crack front profiles that are revealed in our measurements indicate that the concept of energy

balance must be extended to include crack front shapes and dynamics, as suggested by Eq. (1). This is true not only for stepped cracks, where explicit h -dependent contributions to $l(t)$ must be accounted for, but even for “simple” cracks since their curvature in the xz plane is nontrivial [as Figs. 1(c) and 3(c) show]. So long as measurements of G are performed at sufficient distances from the crack plane(s), however, the effective 2D approach inherent in the use of the J -integral is still valid [see Figs. 3(b) and S3].

In conclusion, we have found two explicit conditions for a transition from stepped to simple crack to occur: (1) one needs to momentarily break the topological constraint that enforces a step, and (2) the in-plane front length must be at least as long as that of a simple crack. Energy balance is therefore a necessary, but not a sufficient condition for a simple crack to propagate. Below the minimum v_s in Fig. 4(d), G is sufficient to enable propagation of simple crack, but the stepped crack dynamics prefer to cause a crack to arrest [25], instead of allowing the transition to simple cracks to occur. Hence, we see that 3D fracture dynamics require more complex conditions than the “simple” condition of energy balance that governs “2D” crack dynamics.

When considering step dynamics and structure, crack inertia should be irrelevant as $v \ll c_R$. We have, however, demonstrated that 3D structure and dynamics of these cracks is still quite complex. Understanding these intriguing questions poses numerous nontrivial theoretical challenges, and suggests that “simple” extensions to 2D fracture mechanics may not be sufficient.

M.W. and J.F. gratefully acknowledge the support of the Israel Science Foundation, Grant. No 840/19. This work was supported by the International Research Project “Non-Equilibrium Physics of Complex Systems” (IRP-PhyComSys, France-Israel). M.A.B. and M.W. acknowledge the support of the Lady Davis Fellowship Trust.

-
- [1] L. B. Freund, *Dynamic Fracture Mechanics* (Cambridge University Press, Cambridge, England, 1998).
 - [2] J. Fineberg and M. Marder, Instability in dynamic fracture, *Phys. Rep.* **313**, 1 (1999).
 - [3] E. Bouchbinder, J. Fineberg, and M. Marder, Dynamics of simple cracks, *Annu. Rev. Condens. Matter Phys.* **1**, 371 (2010).
 - [4] I. Kolvin, G. Cohen, and J. Fineberg, Crack Front Dynamics: The Interplay of Singular Geometry and Crack Instabilities, *Phys. Rev. Lett.* **114**, 175501 (2015).
 - [5] T. Goldman, A. Livne, and J. Fineberg, Acquisition of Inertia by a Moving Crack, *Phys. Rev. Lett.* **104**, 114301 (2010).
 - [6] E. Bouchbinder, T. Goldman, and J. Fineberg, The dynamics of rapid fracture: instabilities, nonlinearities and length scales, *Rep. Prog. Phys.* **77**, 046501 (2014).
 - [7] K. Ravi-Chandar and W. Knauss, An experimental investigation into dynamic fracture: II. microstructural aspects, *Int. J. Fract.* **26**, 65 (1984).
 - [8] J. Fineberg, S. P. Gross, M. Marder, and H. L. Swinney, Instability in dynamic fracture, *Phys. Rev. Lett.* **67**, 457 (1991).
 - [9] K. Ravi-Chandar, *Dynamic Fracture* (Elsevier, Amsterdam, 2004).
 - [10] M. Wang, M. Fourmeau, L. Zhao, F. Legrand, and D. Nélias, Self-emitted surface corrugations in dynamic fracture of silicon single crystal, *Proc. Natl. Acad. Sci. USA* **117**, 16872 (2020).
 - [11] O. Ronsin, C. Caroli, and T. Baumberger, Crack front echelon instability in mixed mode fracture of a strongly nonlinear elastic solid, *Europhys. Lett.* **105**, 34001 (2014).
 - [12] K. Pham and K. Ravi-Chandar, On the growth of cracks under mixed-mode I+III loading, *Int. J. Fract.* **199**, 105 (2016).
 - [13] A. J. Pons and A. Karma, Helical crack-front instability in mixed-mode fracture, *Nature (London)* **464**, 85 (2010).
 - [14] C.-H. Chen, T. Cambonie, V. Lazarus, M. Nicoli, A. J. Pons, and A. Karma, Crack Front Segmentation and Facet Coarsening in Mixed-Mode Fracture, *Phys. Rev. Lett.* **115**, 265503 (2015).
 - [15] E. Sommer, Formation of fracture lances in glass, *Eng. Fract. Mech.* **1**, 539 (1969).
 - [16] Y. Tanaka, K. Fukao, Y. Miyamoto, and K. Sekimoto, Discontinuous crack fronts of three-dimensional fractures, *Europhys. Lett.* **43**, 664 (1998).

- [17] T. Baumberger, C. Caroli, D. Martina, and O. Ronsin, Magic Angles and Cross-Hatching Instability in Hydrogel Fracture, *Phys. Rev. Lett.* **100**, 178303 (2008).
- [18] I. Kolvin, G. Cohen, and J. Fineberg, Topological defects govern crack front motion and facet formation on broken surfaces, *Nat. Mater.* **17**, 140 (2018).
- [19] M. Wang, M. Adda-Bedia, J. M. Kolinski, and J. Fineberg, How hidden 3d structure within crack fronts reveals energy balance, *J. Mech. Phys. Solids* **161**, 104795 (2022).
- [20] T. G. Boué, R. Harpaz, J. Fineberg, and E. Bouchbinder, Failing softly: a fracture theory of highly-deformable materials, *Soft Matter* **11**, 3812 (2015).
- [21] A. Livne, G. Cohen, and J. Fineberg, Universality and Hysteretic Dynamics in Rapid Fracture, *Phys. Rev. Lett.* **94**, 224301 (2005).
- [22] Y. Hu and Z. Suo, Viscoelasticity and poroelasticity in elastomeric gels, *Acta Mechanica Solida Sinica* **25**, 441 (2012).
- [23] C. Li, Z. Wang, Y. Wang, Q. He, R. Long, and S. Cai, Effects of network structures on the fracture of hydrogel, *Extreme Mech. Lett.* **49**, 101495 (2021).
- [24] S. Hassan, J. Kim *et al.*, Polyacrylamide hydrogels. iv. near-perfect elasticity and rate-dependent toughness, *J. Mech. Phys. Solids* **158**, 104675 (2022).
- [25] See Supplemental Material at <http://link.aps.org/supplemental/10.1103/PhysRevResearch.5.L012001> for details of fracture experiments surrounded by water, simple crack front shapes, evolution of in-plane crack front length of stepped crack fronts during the multiple step reflections, and how the internal structures within the stepped crack front lead to the crack arrest. The material includes Refs. [11,24].
- [26] G. Noselli, A. Lucantonio, R. M. McMeeking, and A. DeSimone, Poroelastic toughening in polymer gels: A theoretical and numerical study, *J. Mech. Phys. Solids* **94**, 33 (2016).
- [27] Y. Yu, C. M. Landis, and R. Huang, Steady-state crack growth in polymer gels: A linear poroelastic analysis, *J. Mech. Phys. Solids* **118**, 15 (2018).
- [28] R. Long and C.-Y. Hui, Fracture toughness of hydrogels: measurement and interpretation, *Soft Matter* **12**, 8069 (2016).
- [29] A. Livne, E. Bouchbinder, I. Svetlizky, and J. Fineberg, The near-tip fields of fast cracks, *Science* **327**, 1359 (2010).
- [30] T. G. Boué, G. Cohen, and J. Fineberg, Origin of the Microbranching Instability in Rapid Cracks, *Phys. Rev. Lett.* **114**, 054301 (2015).
- [31] P. S. Theocaris, Local yielding around a crack tip in plexiglas, *J. Appl. Mech.* **37**, 409 (1970).
- [32] Y. Morishita, K. Tsunoda, and K. Urayama, Velocity transition in the crack growth dynamics of filled elastomers: Contributions of nonlinear viscoelasticity, *Phys. Rev. E* **93**, 043001 (2016).
- [33] Y. Tanaka, K. Fukao, and Y. Miyamoto, Fracture energy of gels, *Eur. Phys. J. E* **3**, 395 (2000).